Absolute calibration of Fujifilm BAS-TR image plate response to laser driven protons up to 40 MeV

P. Martin, H. Ahmed, D. Doria, A. Alejo, R. Clarke, S. Ferguson, J. Fernández-Tobias, R. Freeman, J. Fuchs, A. Green, et al.

Absolute calibration of Fujifilm BAS-TR image plate response to laser driven protons up to 40 MeV

P. Martin,[1, a)] H. Ahmed,[1, 2] D. Doria,[1, 3] A. Alejo,[1, 4] R. Clarke,[2] S. Ferguson,[1] J. Fernández-Tobias,[2, 5] R. R. Freeman,[6] J. Fuchs,[7] A. Green,[1] J. S. Green,[2] D. Gwynne,[1] F. Hanton,[1] J. Jarrett,[8] D. Jung,[1] K. F. Kakolee,[1, 9] A. G. Krygier,[6] C. L. S. Lewis,[1] A. McIlvenny,[1] P. McKenna,[8] J. T. Morrison,[10] Z. Najmudin,[11] K. Naughton,[1] G. Nersisyan,[1] P. Norreys,[12] M. Notley,[2] M. Roth,[13] J. A. Ruiz,[5] C. Scullion,[1] M. Zepf,[14, 15, 16] S. Zhai,[1, 17] M. Borghesi,[1] and S. Kar[1, b)]

[1)] *Centre for Plasma Physics, School of Mathematics and Physics, Queen's University Belfast, Belfast BT7 1NN, United Kingdom*

[2)] *Central Laser Facility, Rutherford Appleton Laboratory, Didcot, Oxfordshire OX11 0QX, United Kingdom*

[3)] *Extreme Light Infrastructure (ELI-NP), and Horia Hulubei National Institute for R&D in Physics and Nuclear Engineering (IFIN-HH), Str. Reatorului No. 30, 077125 Bucharest-Magurele, Romania*

[4)] *IGFAE, Universidade de Santiago de Compostela, 27002 Santiago de Compostela, Spain*

[5)] *Instituto de Fusion Nuclear, Universidad Politécnica de Madrid, 28040 Madrid, Spain*

[6)] *Department of Physics, The Ohio State University, Columbus, Ohio 43210, USA*

[7)] *LULI - CNRS, CEA, UPMC Univ Paris 06 : Sorbonne Université, Ecole Polytechnique, Institut Polytechnique de Paris - F-91128 Palaiseau cedex, France*

[8)] *Department of Physics, SUPA, University of Strathclyde, Glasgow G4 0NG, United Kingdom*

[9)] *Department of Physics, Jagannath University, Dhaka-1100, Bangladesh*

[10)] *Department of Electrical and Computer Engineering, Colorado State University, Fort Collins, CO 80523, USA*

[11)] *Blackett Laboratory, Department of Physics, Imperial College, London SW7 2AZ, United Kingdom*

[12)] *Department of Physics, University of Oxford, Oxford OX1 3PU, United Kingdom*

[13)] *Institut für Kernphysik, Technische Universität Darmstadt, Schloßgartenstrasse 9, 64289 Darmstadt, Germany*

[14)] *Helmholtz Institut Jena, 07743 Jena, Germany*

[15)] *Institute for Quantumoptics, University of Jena, 07743 Jena, Germany*

[16)] *GSI GmbH, 64291 Darmstadt, Germany*

[17)] *Department of Mathematics and Physics, Shanghai Normal University, Shanghai 200234, China*

Image plates (IPs) are a popular detector in the field of laser driven ion acceleration, owing to their high dynamic range, and reusability. An absolute calibration of these detectors to laser-driven protons in the routinely produced tens of MeV energy range is therefore essential. In this paper, the response of Fujifilm BAS-TR IPs to 1–40 MeV protons is calibrated by employing the detectors in high resolution Thomson parabola spectrometers, in conjunction with CR-39 nuclear track detector to determine absolute proton numbers. While the CR-39 was placed in front of the image plate for lower energy protons, it was placed behind the image plate for energies above 10 MeV, using suitable metal filters sandwiched between the image plate and CR-39 to select specific energies. The measured response agrees well with previous reported calibrations, as well as standard models of IP response, providing, for the first time, an absolute calibration over a large range of proton energies of relevance to current experiments.

I. INTRODUCTION

The use of high power laser drivers is a well established method of generating high energy, short duration bursts of ions[1]. These ion sources have several favourable properties over conventionally accelerated ion beams, such as their shorter bunch duration (ps–ns)[2], high laminarity and low emittance[3,4], and high particle number. For these reasons, laser driven proton beams have been investigated for use in various applications, such as radiobiology physics[5,6], warm dense matter[7], fast ignition[8], and proton radiography[9,10].

Much of the initial research was focused on the target normal sheath acceleration[11] (TNSA) mechanism using micron-scale thick targets. TNSA generates an exponentially decaying ion spectrum, and favours the acceleration of high charge-mass ratio ions (such as protons).

[a)] Corresponding author: p.martin@qub.ac.uk

[b)] Electronic mail: s.kar@qub.ac.uk

This mechanism has been demonstrated experimentally to generate protons of up to 85 MeV[12], however, advances in ultrathin target manufacturing have enabled the possibility of using targets in the tens of nm scale thickness, and as such has seen the emergence of new mechanisms, such as radiation pressure acceleration (RPA)[1,13,14], and acceleration enhanced by relativistically induced transparency (RIT)[15,16]. These new mechanisms have extended the highest proton energies achieved thus far to almost 100 MeV[17]. Current experiments are moving towards the generation of higher energy beams, and modern PW-class laser facilities routinely produce protons several tens of MeV in energy[18]. Most laser driven ion acceleration experiments make use of a suite of diagnostics to determine the ion dynamics, such as stacks of radiochromic film (RCF), and Thomson parabola spectrometers (TPS) to measure energy spectra of the ions generated in the interaction[19]. TPS are often employed in laser ion acceleration experiments because they offer higher spectral resolution, as well as the ability to discriminate ion species according to their charge-mass ratio, which is useful considering the multispecies nature of most laser-generated ion beams. The TPS is usually coupled with a particle detector that has been calibrated to determine absolutely the particle number at each energy.

Common detectors coupled with a TPS include CR-39 nuclear track detector, micro-channel plate (MCP) detectors, and image plates (IPs). CR-39 has the advantage that it can detect single particle interactions[20], and therefore does not require prior calibration for use as a detector. However, the etching process which makes the ion damage tracks visible can be long, and may not be an efficient detection method when taking many shots in an experimental campaign. MCP detector assemblies in a TPS consist of a microchannel plate, coupled to a phosphor screen. The ion traces which appear on the phosphor screen are then imaged by a camera at the rear of the detector. These detectors are, in contrast to CR-39, much more efficient in experiments with a high shot rate, however the equipment is expensive, delicate (MCPs must be kept continuously under vacuum and operate at high voltages, which means they can be affected by the large electromagnetic pulses (EMPs) generated in high power laser interactions), and there has been comparatively limited research in calibrating these detectors to the many different ion species produced in experiments with high power lasers[21–23]. Image Plates relying on photo-stimulated luminescence (PSL) are amongst the most popular and reliable detectors used currently for laser driven particle acceleration experiments. This is due to their high dynamic range, low cost as compared to MCPs, relative fast scanning and analysis compared to CR-39, and their ability to be erased with a bright white light source and reused continuously, provided the active phosphor layer remains undamaged.

Currently, the majority of experimentally measured IP response calibrations, specifically for the BAS-TR brand most commonly used in ion acceleration experiments, are to low energy protons (<3 MeV)[24–27], and there is a significant difference in opinion about the response at these low energies between the different works (up to a factor of 2). In addition, the only works that have a response in energy ranges relevant to current experimental efforts either do not use an absolute reference for determining proton number[24], or utilise a conventionally accelerated proton source[28].Thus, there exists a gap in the literature for a calibration of IP response to laser-driven protons at energies that are applicable to modern experiments with high power lasers. In this paper, a calibration of the response of BAS-TR IPs to laser driven protons in the energy range 1–40 MeV is presented, using CR-39 detectors as an absolute reference for particle number. A short summary of the previous efforts to calibrate BAS-TR IPs is given, followed by a description of our experimental setup, and a new high energy implementation of an image plate calibration using CR-39 is demonstrated. The new experimentally measured response is compared to the previous works, and a fitting of our data to IP response models presented by other groups is performed, together with an empirical function for extrapolation to high energies.

II. IMAGE PLATES: SIGNAL REGISTRATION AND FADING

IPs are composed of an active phosphor layer on top of a magnetic base. The Fujifilm BAS-SR and BAS-MS brands of image plate also have a protective layer over the active layer, however the BAS-TR, which is the on discussed in this article, does not. The BAS-TR brand is the one most commonly used in laser ion acceleration studies, because there is no loss of data due to lower energy ions stopping in the protective layer before reaching the active layer. The active layer of the BAS-TR brand is composed of 50 μm thick europium doped barium fluoride phosphor, with the chemical formula $BaFBr_{0.85}I_{0.15} : Eu^{2+}$, and at a density of 2.85 g/cm^3[25]. When ionizing radiation is incident on the active layer, the above molecule is promoted to an excited, metastable state which can persist for several hours. The state can decay either via spontaneous emission or by stimulated emission when irradiated by light at an appropriate wavelength. Image plate scanners (such as the Fujifilm FLA-5000 used in this paper) use 635 nm, 45 mW laser radiation to stimulate the emission of 400 nm photons, which are detected and recorded in the scanner as a pixel value, known as quantum level (QL). This quantum level must be converted into a PSL value before analysis, according to a formula as given by Fujifilm[29,30]:

$$PSL = \left(\frac{R}{100}\right)^2 \times \frac{4000}{S} \times 10^{L\left(\frac{QL}{2^G-1}-\frac{1}{2}\right)}, \qquad (1)$$

where R is the scanning resolution, S is the scanner sensitivity, L is the latitude, and G is the bit depth. In this

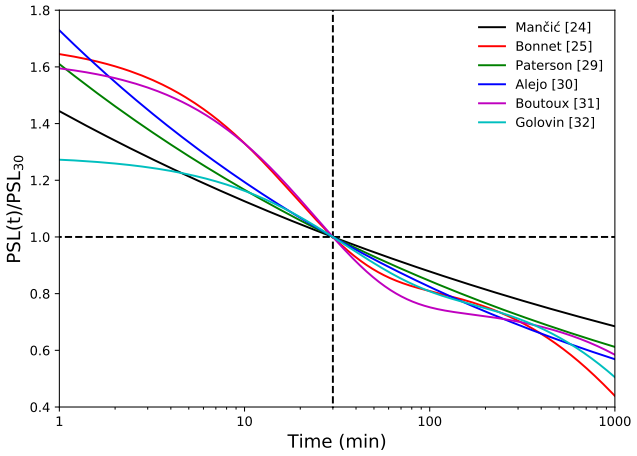

FIG. 1. Comparison of different fading functions from Mančić *et al.*[24], Bonnet *et al.*[25], Paterson *et al.*[29], Alejo *et al.*[30], Boutoux *et al.*[31], and Golovin *et al.*[32]. The functions given by each group have been converted into the formula for $PSL(t)/PSL_{30}$, for consistency with the chosen convention for this work and to aid comparisons.

experiment, these values were $R = 25$ μm, $S = 5000$, $L = 5$, and $G = 16$. It is this PSL value that must be experimentally calibrated to determine the absolute particle number, as a function of the particles incident energy.

Due to spontaneous decay of the metastable state, the signal intensity on an image plate will fade exponentially over time. This means the PSL signal read on the scanner must be corrected for the time taken between IP irradiation and scanning. Several groups have reported their experimentally determined fading functions for the PSL signal[24,25,29–32]. The fading curve is characterised by a very fast decay in the first 20–30 minutes after irradiation, which transitions to a slower decay for long wait times. The signal fading must be corrected relative to a given time at which the response function is evaluated. As such, the convention adopted by Refs.[30,33,34], will be used for this paper, which used the PSL signal 30 minutes after irradiation, henceforth referred to as PSL_{30}. The function used in this paper to correct the PSL signal measured t minutes after exposure to PSL_{30}, is[30]:

$$PSL_{30} = \left(\frac{30}{t}\right)^{-0.161} PSL(t) \tag{2}$$

A comparison of the various other fading functions (which each have been converted from their original form to the factor $PSL(t)/PSL_{30}$ for ease of comparison) is shown in Figure 1. As can be seen, the largest deviations of each function from each other occurs in the early stages after irradiation, thus it is good practice to wait for longer than 30 minutes before scanning the IP, in order to minimise potential errors by comparing results between experiments that could be introduced by the use of a different fading function.

III. PREVIOUS WORKS ON IP RESPONSE TO MULTI-MEV PROTONS

The response of BAS-TR IPs to protons has been shown before by several groups, using different methods. The measured responses from these works is shown in Fig. 2, where each groups data has been fading corrected to the PSL_{30} convention, using the fading functions specified in each work. The legend in Fig. 2 indicates the facility used in each work, as well as the method used to determine proton number incident on the IPs (in brackets). Bonnet *et al.*[25] and Freeman *et al.*[26] determined the response using conventional accelerators up to an energy of ∼3 MeV. Rabhi *et al.*[28] used two conventional accelerators: The CPO facility, where they measured the response of protons in the range 80–200 MeV, and the ALTO-Tandem facility, where for the TR branded IP they only reported the measurement for a single energy, ∼2 MeV. In the work from Bonnet *et al.*, Rutherford back scattering (RBS) off a tantalum target was used to irradiate the IPs, and a silicon diode detector placed at the opposite backscatter angle to the IP. Due to the nature of Rutherford scattering, the two equal and opposite angles should receive the same average proton flux. Uncertainty using this method is dominated by the systematic error in determining the solid angle subtended by the detector from the target. For the other works employing conventional accelerators, the flux incident on the IP was determined with beam charge/current monitors. In contrast, Mančić *et al.*[24] used laser-driven protons (from the LULI facility) up to an energy of 20 MeV. While the IP response for low energies (up to 2 MeV) was obtained by using CR-39 nuclear track detector, for higher energies, they inferred the proton number incident on the IP from dose measurements on RCF. Dose is typically calculated through the use of a function of the film's optical density, which itself needs to be calibrated. This method of calculating proton number using RCF introduces an additional source of systematic error in the IP response calculation.

In order to determine the IP response, some groups have fit functions to the experimental data, as in Refs.[24,30,33], while others[25,38,39] have attempted to create models of the response, based on energy deposited in the active layer by the protons, E_{Dep}. The response of IPs to protons was first modelled by Bonnet *et al.*[25], who directly related the response to the deposited energy by the equation:

$$PSL/p^{+} = \alpha \int_0^w \frac{dE}{dz} \exp\left(-\frac{z}{L}\right) dz, \tag{3}$$

where PSL/p^{+} is the PSL per incident proton immediately after exposure, α is an experimentally measured sensitivity factor, w is the thickness of the active layer, dE/dz is the linear energy transfer (LET) of the protons of energy E, z is the depth into the active layer, and L is a characteristic absorption length, dependent

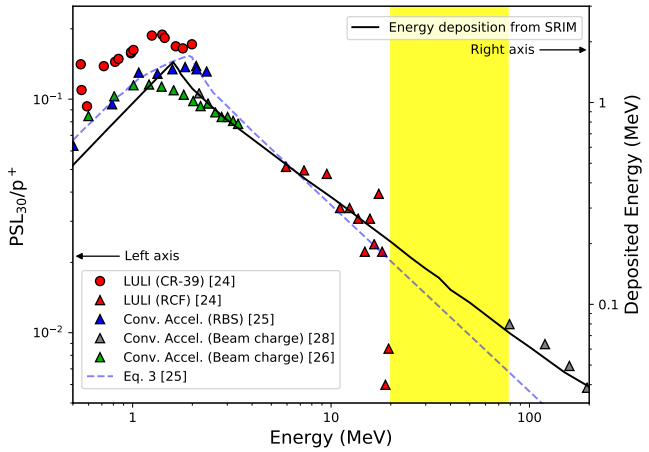

FIG. 2. **Left axis**: Comparison of the experimentally measured responses (converted to PSL_{30} per proton, using the fading functions and times specified in each work) by Mančić *et al.*[24], Bonnet *et al.*[25], Rabhi *et al.*[28], and Freeman *et al.*[26]. The legend indicates the proton source for each data set, as well as the method used to determine proton number incident on the IPs (in brackets). The yellow region represents the energy range in which no calibration data has been reported. The blue dashed line represents the response curve given by Eq. (3), as determined by Bonnet *et al.*[25], using values for their reported parameters[35]. **Right axis**: Energy deposited by protons in the active layer, E_{Dep}, obtained from SRIM simulations[36,37] (black line). A peak in the energy deposition is observed at ∼1.6 MeV.

on the type of IP, scanner, and scanning laser parameters, determined to be 44 ± 4 μm for BAS-TR IPs[35]. The exponential factor is included to account for absorption of the PSL photons in the active layer before they escape and are detected. In order to compute the energy lost by the protons in the active layer, simulations were ran using the Monte Carlo SRIM[36,37] software, which is shown on the right-side y axis in Figure 2. The calculated response using the values of α and L from Ref.[35] is shown as the blue dashed line in Fig. 2. A broad agreement with the experimental data can be seen in the energy range investigated (<3 MeV), however when extrapolating to higher energies the response is significantly underestimated compared to the experimental data reported by Rabhi *et al.*[28] using a conventional accelerator. Lelasseux *et al.*[38] built on the work by Bonnet and that of Birks[40] to describe a new function, taking into account saturation of the active medium:

$$PSL/p^{+} = \alpha \int_{0}^{w} \frac{\frac{dE}{dz} \exp\left(-\frac{z}{L}\right)}{1 + kB\frac{dE}{dz}} dz, \qquad (4)$$

where kB is a quenching factor, given by Lelasseux as 0.15 Angstrom/eV for BAS-TR IPs. The sensitivity parameter, α, on the other hand, was estimated by fitting Eq. (4) to the available experimental data. However, it is worth noting that differences in fading conventions between different experimental data sets were not taken into account in their attempt to fit the data in Ref.[38], and as a result likely underestimate the value of α required for fitting. Nishiuchi *et al.*[39] proposed a model based on Eq. (4), but with a second sensitivity term, α_2, added in the integrand, which accounts for high-LET radiation:

$$PSL/p^{+} = \int_{0}^{w} \frac{dE}{dz} \left(\frac{\alpha \exp\left(-\frac{z}{L}\right)}{1 + kB\frac{dE}{dz}} + \alpha_2 \right) dz. \qquad (5)$$

For relatively low-LET radiation, such as protons, the value of this second term is expected to be significantly lower than the first term, and thus, the model reduces to Eq. (4).

While there is broad agreement between previous efforts to calibrate BAS-TR IPs both theoretically and experimentally, there still exists some uncertainty in the true response, and different works deviate from one another. First, the experimental data for low energies has a significant (up to factor of 2) variation, which makes the attempt to make a reliable fit by the theoretical models difficult. Secondly, there is a significant gap in experimental data in the 10s of MeV range, while the data points between 5–20 MeV are obtained by a less accurate method and 80–200 MeV were obtained using conventional accelerator rather than laser-driven protons. As a result, a coherent and absolute calibration of the IP response over a broad energy range is missing, which is necessary to both corroborate experimental data and to fine tune parameters of the response models. An absolute calibration of IP response to laser driven protons in the range of energies most relevant to current experiments is obtained by deploying CR-39 in different configurations with the IP, as discussed below.

IV. EXPERIMENTAL SETUP

The data shown in this paper was collected from three experimental campaigns, two at the petawatt target area of the Vulcan laser system, located at the Central Laser Facility in the UK, and the third at the TARANIS laser system, situated in Queen's University Belfast. The campaigns were primarily focused on laser driven ion acceleration from thin foils, however a limited number of IP calibration shots were performed in each case. The Vulcan laser pulse of 600–900 fs duration and ∼190 J energy on target was focused using an $f/3$ off-axis parabola, to a spot of ∼5 μm full width at half maximum (FWHM) diameter, after reflection off a plasma mirror. Using these values, a peak on target intensity of $(3-5) \times 10^{20}$ W/cm^2 was estimated in both campaigns at Vulcan. The pulse was focused at near-normal incidence onto plastic (CH) targets, ranging from 50 nm up to 10 μm in thickness, accelerating the carbon and protons present to high energy. The TARANIS laser system[41] delivered pulses ∼600 fs in duration, at intensities on the order of 10^{19} W/cm^2, onto

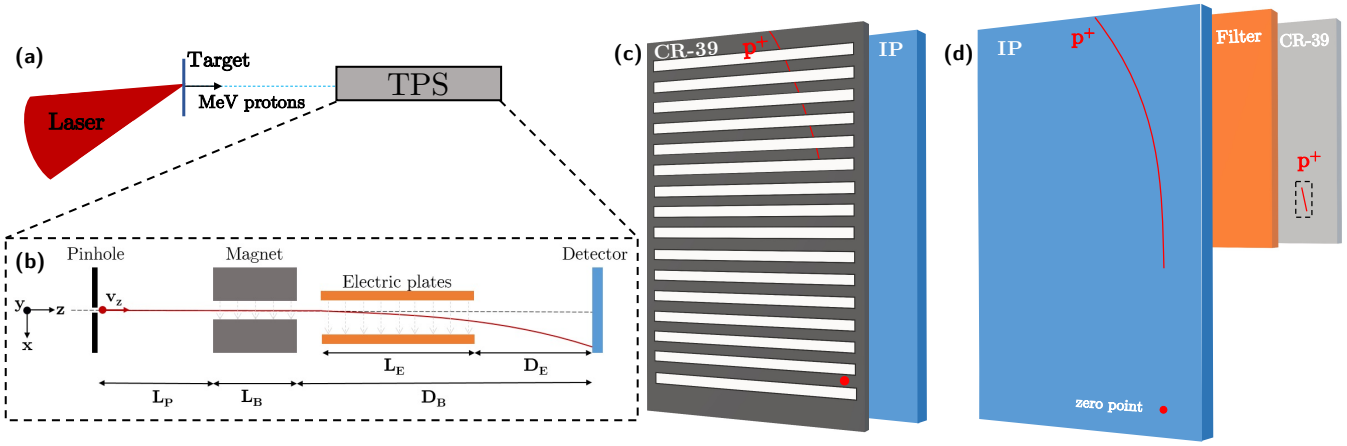

FIG. 3. (a) Schematic of a typical experimental setup used at each laser system. (b) Schematic of a Thomson parabola spectrometer. (c) Slotted CR-39/IP detector assembly used to calibrate low energy (sub-10 MeV) protons in Experiments 1 and 2 listed in Table I. (d) The layout of the IP/filter/CR-39 detector assembly from Experiment 3 for the calibration of protons above 10 MeV.

$\sim$10 μm thick Al targets, producing protons at energies of several MeV. For the IP calibration, Thomson parabola spectrometers, coupled with an IP as the primary particle detector were used. A schematic of the experimental setup at these campaigns is shown in Figure 3(a), and a description of the details of each experiment is listed in Table I, with each experiment assigned a number from 1–3 for referencing later. TPS are spectrometers which use magnetic and electric fields to separate charged particles according to their energy, as well as their charge-mass ratio (q/m). The ions form a parabolic trace along the detector plane, with their x and y positions with respect to zero deflection determined by (6) and (7).

$$y = \frac{q}{mv_z} B_0 L_B \left(\frac{L_B}{2} + D_B \right), \tag{6}$$

$$x = \frac{q}{mv_z^2} E_0 L_E \left(\frac{L_E}{2} + D_E \right), \tag{7}$$

where q is the ion charge, m is the mass, v_z is the velocity, B_0 and E_0 are the magnetic and electric field strengths, respectively, and L_B, L_E, D_E, and D_B are the distances as defined in Figure 3(b). Thus, the vertical distance on the detector above the zero point will determine the energy of the ion, the PSL value of which can be easily extracted. In order to determine the number of protons at that point, CR-39 can be used in conjunction with the IP. CR-39 is a solid state detector that, when etched in a sodium hydroxide (NaOH) bath for a certain time, will display the ion damage tracks that are then visible through a microscope[20,42], and can be counted manually or by using image analysis software.

The visibility of the etched pits in the CR-39 depends on the LET of the particle entering it, and due to the nature of the Bragg peak that is characteristic of ion stopping in matter, most of the ions kinetic energy is lost at the end of its trajectory. Thus, ion damage tracks in CR-39 are usually only visible if the ion fully stops inside the material. For the 1 mm thick CR-39 used in this work, protons below $\sim$10 MeV stop inside the detector. Therefore, for protons of energies below 10 MeV, a slotted piece of CR-39 was placed in front of the IP in experiments 1 and 2, as used in Refs.[22,23,27,30,33,43] and shown in Fig. 3(c). In this case, the PSL values immediately adjacent to the edges of the CR-39 slots could be integrated across the proton trace. The proton pits at the CR-39 edge would then be binned into areas of the same size as the sampling interval on the scanned IP (25 μm), and integrated across the slot edge. This enables a direct comparison between PSL and the number of pits counted at the slot edges, to provide a value of the PSL per incident proton at that energy. This technique has been used in the past successfully for the calibration of low energy (<0.2 MeV) protons[27], as well as deuterium[30], carbon[27,33], titanium[34], and gold[44] ions.

For the calibration of higher energy protons, it would not be possible to use CR-39 in front of the IP. Therefore, in Experiment 3 CR-39 were used behind the IP with a suitable thickness of iron or copper filter in between, as shown in Fig. 3(d). The filter reduces the energies of the transmitted protons to below 10 MeV, in order for them to stop in the CR-39 and be visible after etching. The range of energies which could be detected at the front and back surfaces of the CR-39 with a set of filters, as listed in Table II, was determined through SRIM simulations.

The minimum and maximum energies shown in Table II determine the energy range of protons which will show up in CR-39 after etching, resulting in a “streak” of pits that aligns with a small section of the proton trace on the IP. The CR-39 was etched in a NaOH solution at a concentration of 6.5 mol/kg at 85°C for up to 80 minutes, and the pits counted on both the front and back surfaces. An image of the streak of proton pits on a CR-39 is shown in Fig. 5 along with the image of the IP from the same

Experiment no.	Laser system	I_0 (W/cm^2)	Target	Proton energy range (MeV)	Calibration method
1	TARANIS	$\sim 10^{19}$	10 μm Al	1.5–2.1	Slotted CR-39 + IP
2	Vulcan	$(3-5)\times 10^{20}$	10 μm CH	3.6–10.6	Slotted CR-39 + IP
3	Vulcan	$(3-5)\times 10^{20}$	50 nm CH	13.2–40.3	IP + filter + CR-39

TABLE I. Details of the three experiments described in this paper, including the laser system used, peak intensity (I_0), and types of target shot, together with the energy range of protons investigated for the IP calibration and the detector assembly setup in each.

shot. The proton streaks on CR-39 were all binned into approximately equal sized sections, 600–800 μm long and ~350 μm wide (the full trace width). Lateral straggling of the protons while passing through the IP-filter assemblies was determined using SRIM to be ~10 μm at the lowest energies (in the case of the 250 μm Cu filter), to ~90 μm at the highest energy (2500 μm Fe). Therefore the straggling can be considered to be small compared to the size of the bins, as well as the energy resolution of the TPS, which is determined by the TPS geometry and pinhole diameter[45] (250 μm). Fig. 4 shows the outputs from SRIM for protons passing through an image plate and 1250 μm Cu filter. The lateral straggle of protons that reach the front surface of the CR-39 is measured to be ~70 μm. This value is in line with the measured increase in trace width between the IP and CR-39 pit streak shown in Fig. 5. Knowing the minimum proton energy reaching the front surface of the CR-39, and the maximum energy stopping at the rear surface, one can, using Eqs. (6) and (7), calculate the central energy of each bin in the CR-39, and its corresponding energy bandwidth from the bin width. The PSL signal on the IP was then integrated (after background subtraction) across each energy range calculated for the bins, as shown in Fig. 5(c), and divided by the number of pits, to give the PSL per proton for that energy bin.

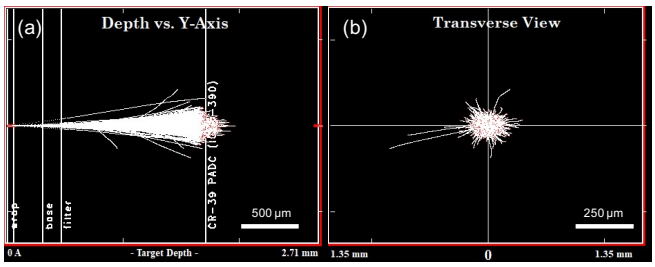

FIG. 4. Outputs from a SRIM simulation of the detector assembly in Fig. 3(d), using 1250 μm Cu filter and 27.4 MeV incident proton energy, corresponding to the data shown in Fig. 5(a). Scale bars are shown in the bottom right corners. (a) Trajectories of 27.4 MeV protons in the Y-Z plane (Z is direction of travel). (b) Transverse (X-Y) distribution of the protons on the CR-39 front surface, where the lateral straggle of the protons is calculated as ~70 μm.

Filter	Min Energy (MeV)	Max Energy (MeV)
250 μm Cu	13.2	17.6
500 μm Cu	17.6	21.3
1250 μm Cu	27.4	30.2
2500 μm Fe	38.1	40.3

TABLE II. Filters used for the calibration of high energy protons, and the lower and upper limits of the proton energies (before filtration) which allow observation of the pits in the CR-39 after etching, as determined through SRIM.

V. EXPERIMENTAL RESULTS

The calculated response of the IP for the high energy protons from Experiment 3 is plotted in Fig. 6, alongside the low energy data obtained in Experiments 1 and 2 using the slotted CR-39. In Figure 6(a), the data is plotted with data from previous works[24–26,28] (also shown in Fig. 2). It can be seen that there is a good agreement overall between data sets, with the trends laid out by the other works. In the low energy (few-MeV) range, our data fits best with that of Mančić *et al.*[24], who is the only other group using CR-39, and laser-driven protons. However, at higher energies the data from Mančić shows some large deviations compared to our measured response. As mentioned above, this could be due to the fact that Mančić *et al.*[24] deduced the proton numbers for energies above 2 MeV from dose measurements on RCF, which may have introduced an additional source of systematic errors to the response. The consistency in the trend of our data points over a wide range of energies from 1–40 MeV suggests a more reliable IP response for protons that can be extended to higher energies in line with the data points given by Rabhi *et al.*[28].

One can use the models described by the other groups (Eqs. (3) and (4)), and a least squares fitting to our data to find new values of the sensitivity parameter, α. From the Bonnet model, Eq. (3), the value of the sensitivity (and associated one standard deviation error) was determined to be $\alpha = 0.41 \pm 0.01$ PSL/MeV. This is in agreement with the same value determined by Rabhi *et al.* ($\alpha = 0.4 \pm 0.04$ PSL/MeV)[28], however differs significantly to what was calculated by Bonnet ($\alpha = 0.247 \pm 0.007$ PSL/MeV)[35]. This is most likely due to the small energy range investigated by Bonnet, which their model

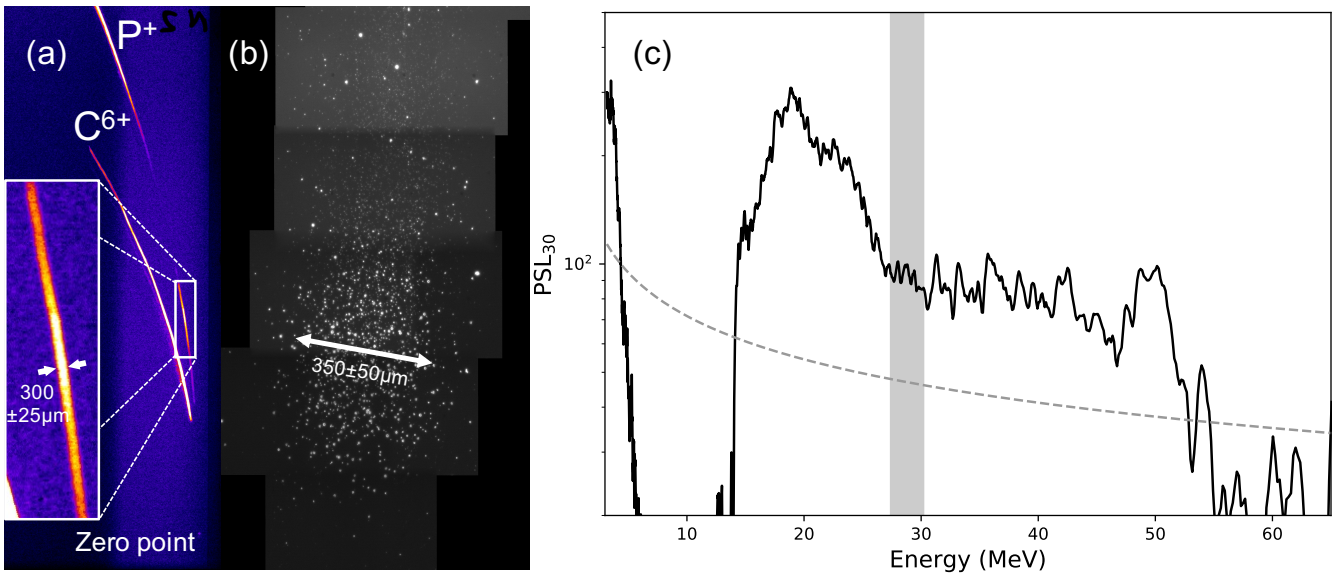

FIG. 5. (a) Scanned IP image converted to PSL, with each trace corresponding to ions with a specific q/m labelled. The inset shows a zoomed in portion of the proton trace, which was measured to be (300 ± 25) μm wide. Behind the IP was a 1250 μm Cu filter and CR-39. (b) Microscope image of the proton pits on the front surface of the CR-39 after etching at $\times 20$ magnification. The width of the pit streak was measured to be $\sim(350 \pm 50)$ μm. (c) Background subtracted PSL_{30} profile across the proton trace in the IP shown in (a). The shaded region indicates the energy range which the CR-39 detected protons. The detection limit of the IP is shown as the dashed grey line.

fits reasonably well, but deviates from the observed true response at high energies.

From the model described by Lelasseux *et al.*[38], using their value for $kB = 0.15$ Å/eV, the least squares fitting gave a value of $\alpha = 0.5 \pm 0.01$ PSL/MeV. However, the fitting of this curve did not match well with our lower energy data. In order to improve the accuracy of the model, a least squares fitting was performed while varying both α and kB. This gave a new set of values of the model parameters as $\alpha = 0.44 \pm 0.02$ PSL/MeV, and $kB = 0.04 \pm 0.03$ Å/eV. Our new value of kB is significantly smaller than that originally proposed by Lelasseux, and has a large relative error, which suggests that the contribution of phosphor quenching to the IP response can be lower than originally anticipated. The curves generated by these new values are shown in Fig. 6(b), showing a good agreement between the models and our experimental data.

Using these models require running Monte Carlo simulations to determine proton energy deposition in the active layer. In lieu of this, one may prefer using a best fit function to the data shown in Fig. 6(b), which gives two power laws with different energy limits:

$$PSL_{30}/p^{+} = \begin{cases} 0.151\ E_p^{0.6} & (\mathrm{E_p} < 1.6\ \mathrm{MeV}) \\ 0.284\ E_p^{-0.75} & (\mathrm{E_p} \geq 1.6\ \mathrm{MeV}) \end{cases}, \quad (8)$$

where E_p is the proton energy given in MeV. As there are no experimental data for energies below 1.6 MeV (corresponding to the peak in energy deposition in the active layer — see Fig. 2), the response equation was determined by fitting to the data reported by other works (down to 0.5 MeV), shown in Fig. 6(a), while ensuring a smooth transition between the two parts of Equation (8) at 1.6 MeV.

VI. CONCLUSIONS

The response of Fujifilm BAS-TR image plates to laser-driven protons has been absolutely calibrated up to 40 MeV, the range of energies relevant to current research activities using petawatt-class lasers. Proton numbers were determined using CR-39 nuclear track detectors across the entire energy range, using slotted CR-39 placed in front of the IP for low (<10 MeV) energies, and placed behind the IP with various Fe and Cu filters for high energies. The response, which is in broad agreement with previous works, has been described in terms of the existing models and an empirical fitting as a function of the incident proton energy has been deduced. As the BAS-TR brand of IP is a very popular detector employed, for example, in Thomson parabola spectrometers, this calibration will prove useful in determining accurately proton spectra from future high power laser acceleration experiments.

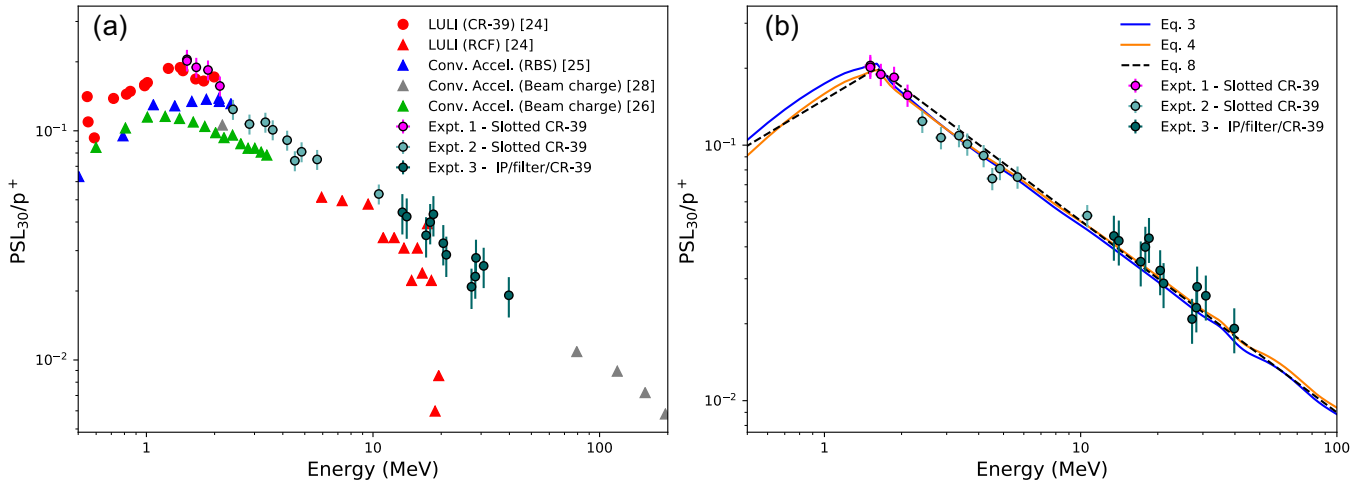

FIG. 6. (a) The calculated IP response data from the experiments described in this work, as labelled in Table I, compared to the experimental data reported by previous works as shown in Figure 2. Vertical error bars represent a ∼10–15% error in counting the pits in the CR-39, and determining the energy ranges over which to integrate the PSL. The errors for data from the slotted CR-39 were smaller, as the PSL in each energy bin could be determined more precisely. Horizontal errors are small, but arise from the width of the energy bins calculated from the CR-39 bins for the high energy data, and for the low energy data using the slotted CR-39 grid, they were determined by the resolution of the TPS. (b) The same experimental data as in (a), fit using the two different models from Eqs. (3), and (4), with newly determined values of the sensitivity parameter, α, and quenching factor, kB, via a least squares fitting. The dashed black line represents the best fit function described by Eq. (8).

ACKNOWLEDGMENTS

The work has been supported by EPSRC (grant EP/K022415/1, EP/J002550/1-Career Acceleration Fellowship held by S.K., EP/L002221/1, EP/K022415/1, EP/J500094/1, and EP/I029206/1). S.Z. acknowledges support by the Chinese Scholarship Council. The authors also acknowledge support from the staff and the target fabrication group at the Central Laser Facility, and G.N. for operating the TARANIS laser in Queen's University Belfast.

[1] A. Macchi, M. Borghesi, and M. Passoni, "Ion acceleration by superintense laser-plasma interaction," Rev. Mod. Phys. **85**, 751–793 (2013), 1302.1775.

[2] B. Dromey, M. Coughlan, L. Senje, M. Taylor, S. Kuschel, B. Villagomez-Bernabe, R. Stefanuik, G. Nersisyan, L. Stella, J. Kohanoff, M. Borghesi, F. Currell, D. Riley, D. Jung, C.-G. Wahlström, C. Lewis, and M. Zepf, "Picosecond metrology of laser-driven proton bursts," Nat. Commun. **7**, 10642 (2016).

[3] M. Borghesi, A. J. Mackinnon, D. H. Campbell, D. G. Hicks, S. Kar, P. K. Patel, D. Price, L. Romagnani, A. Schiavi, and O. Willi, "Multi-mev proton source investigations in ultraintense laser-foil interactions," Phys. Rev. Lett. **92**, 055003 (2004).

[4] T. E. Cowan, J. Fuchs, H. Ruhl, A. Kemp, P. Audebert, M. Roth, R. Stephens, I. Barton, A. Blazevic, E. Brambrink, J. Cobble, J. Fernández, J.-C. Gauthier, M. Geissel, M. Hegelich, J. Kaae, S. Karsch, G. P. Le Sage, S. Letzring, M. Manclossi, S. Meyroneinc, A. Newkirk, H. Pépin, and N. Renard-LeGalloudec, "Ultralow emittance, multi-mev proton beams from a laser virtual-cathode plasma accelerator," Phys. Rev. Lett. **92**, 204801 (2004).

[5] D. Doria, K. F. Kakolee, S. Kar, S. K. Litt, F. Fiorini, H. Ahmed, S. Green, J. C. G. Jeynes, J. Kavanagh, D. Kirby, K. J. Kirkby, C. L. Lewis, M. J. Merchant, G. Nersisyan, R. Prasad, K. M. Prise, G. Schettino, M. Zepf, and M. Borghesi, "Biological effectiveness on live cells of laser driven protons at dose rates exceeding 109 Gy/s," AIP Adv. **2** (2012), 10.1063/1.3699063.

[6] F. Hanton, P. Chaudhary, D. Doria, D. Gwynne, C. Maiorino, C. Scullion, H. Ahmed, T. Marshall, K. Naughton, L. Romagnani, S. Kar, G. Schettino, P. McKenna, S. Botchway, D. R. Symes, P. P. Rajeev, K. M. Prise, and M. Borghesi, "DNA DSB Repair Dynamics following Irradiation with Laser-Driven Protons at Ultra-High Dose Rates," Sci. Rep. **9**, 1–10 (2019).

[7] P. K. Patel, A. J. Mackinnon, M. H. Key, T. E. Cowan, M. E. Foord, M. Allen, D. F. Price, H. Ruhl, P. T. Springer, and R. Stephens, "Isochoric heating of solid-density matter with an ultrafast proton beam," Phys. Rev. Lett. **91**, 125004 (2003).

[8] J. Honrubia, J. Fernández, B. Hegelich, M. Murakami, and C. Enriquez, "Fast ignition driven by quasi-monoenergetic ions: Optimal ion type and reduction of ignition energies with an ion beam array," Laser and Particle Beams **32**, 419–427 (2014).

[9] M. Borghesi, A. Schiavi, D. H. Campbell, M. G. Haines, O. Willi, A. J. MacKinnon, L. A. Gizzi, M. Galimberti, R. J. Clarke, and H. Ruhl, "Proton imaging: a diagnostic for inertial confinement fusion/fast ignitor studies," Plasma Physics and Controlled Fusion **43**, A267–A276 (2001).

[10] L. Romagnani, J. Fuchs, M. Borghesi, P. Antici, P. Audebert, F. Ceccherini, T. Cowan, T. Grismayer, S. Kar, A. Macchi, P. Mora, G. Pretzler, A. Schiavi, T. Toncian, and O. Willi, "Dynamics of electric fields driving the laser acceleration of multi-MeV protons," Phys. Rev. Lett. **95**, 4–7 (2005).

[11] S. C. Wilks, A. B. Langdon, T. E. Cowan, M. Roth, M. Singh, S. Hatchett, M. H. Key, D. Pennington, A. MacKinnon, and R. A. Snavely, "Energetic proton generation in ultra-intense laser-solid interactions," Phys. Plasmas **8**, 542–549 (2001).

[12] F. Wagner, O. Deppert, C. Brabetz, P. Fiala, A. Kleinschmidt, P. Poth, V. A. Schanz, A. Tebartz, B. Zielbauer, M. Roth, T. Stöhlker, and V. Bagnoud, "Maximum Proton Energy above 85 MeV from the Relativistic Interaction of Laser Pulses with Micrometer Thick CH2 Targets," Phys. Rev. Lett. **116**, 1–5 (2016).

[13] T. Esirkepov, M. Borghesi, S. V. Bulanov, G. Mourou, and T. Tajima, "Highly efficient relativistic-ion generation in the laser-piston regime," Phys. Rev. Lett. **92**, 2–5 (2004).

[14] B. Qiao, M. Zepf, M. Borghesi, B. Dromey, M. Geissler, A. Karmakar, and P. Gibbon, "Radiation-pressure acceleration of ion beams from nanofoil targets: The leaky light-sail regime," Phys.

Rev. Lett. **105**, 8–11 (2010).
[15]L. Yin, B. J. Albright, B. M. Hegelich, and J. C. Fernández, "Gev laser ion acceleration from ultrathin targets: The laser break-out afterburner," Laser and Particle Beams **24**, 291–298 (2006).
[16]L. Yin, B. J. Albright, K. J. Bowers, D. Jung, J. C. Fernández, and B. M. Hegelich, "Three-dimensional dynamics of breakout afterburner ion acceleration using high-contrast short-pulse laser and nanoscale targets," Phys. Rev. Lett. **107**, 1–4 (2011).
[17]A. Higginson, R. J. Gray, M. King, N. Butler, R. J. Dance, S. D. R. Willaimson, R. Capdessus, R. Wilson, C. Armstrong, S. J. Hawkes, J. S. Green, P. Martin, W. Q. Wei, X. H. Yuan, S. R. Mirfayzi, S. Kar, R. J. Clarke, D. Neely, and P. McKenna, "Near-100 MeV protons via a laser-driven transparency-enhanced hybrid acceleration scheme," Nat. Commun. **9** (2018), 10.1038/s41467-018-03063-9.
[18]T. Ziegler, D. Albach, C. Bernert, S. Bock, F.-E. Brack, T. E. Cowan, N. P. Dover, M. Garten, L. Gaus, R. Gebhardt, I. Goethel, U. Helbig, A. Irman, H. Kiriyama, T. Kluge, A. Kon, S. Kraft, F. Kroll, M. Loeser, J. Metzkes-Ng, M. Nishiuchi, L. Obst-Huebl, T. Püschel, M. Rehwald, H.-P. Schlenvoigt, U. Schramm, and K. Zeil, "Proton beam quality enhancement by spectral phase control of a PW-class laser system - Scientific Reports," Sci. Rep. **11**, 1–7 (2021).
[19]P. R. Bolton, M. Borghesi, C. Brenner, D. C. Carroll, C. De Martinis, A. Flacco, V. Floquet, J. Fuchs, P. Gallegos, D. Giove, J. S. Green, S. Green, B. Jones, D. Kirby, P. McKenna, D. Neely, F. Nuesslin, R. Prasad, S. Reinhardt, M. Roth, U. Schramm, G. G. Scott, S. Ter-Avetisyan, M. Tolley, G. Turchetti, and J. J. Wilkens, "Instrumentation for diagnostics and control of laser-accelerated proton (ion) beams," Phys. Medica **30**, 255–270 (2014).
[20]S. Kar, M. Borghesi, L. Romagnani, S. Takahashi, A. Zayats, V. Malka, S. Fritzler, and A. Schiavi, "Analysis of latent tracks for MeV protons in CR-39," J. Appl. Phys. **101** (2007), 10.1063/1.2433744.
[21]K. Harres, M. Schollmeier, E. Brambrink, P. Audebert, A. Blažević, K. Flippo, D. C. Gautier, M. Geißel, B. M. Hegelich, F. Nürnberg, J. Schreiber, H. Wahl, and M. Roth, "Development and calibration of a Thomson parabola with microchannel plate for the detection of laser-accelerated MeV ions," Rev. Sci. Instrum. **79**, 093306 (2008).
[22]T. W. Jeong, P. K. Singh, C. Scullion, H. Ahmed, K. F. Kakolee, P. Hadjisolomou, A. Alejo, S. Kar, M. Borghesi, and S. Ter-Avetisyan, "Experimental evaluation of the response of microchannel plate detector to ions with 10s of MeV energies," Rev. Sci. Instrum. **87**, 0–7 (2016).
[23]A. McIlvenny, D. Doria, L. Romagnani, H. Ahmed, P. Martin, S. WIlliamson, E. Ditter, O. Ettlinger, G. Hicks, P. McKenna, Z. Najmudin, D. Neely, S. Kar, and M. Borghesi, "Absolute calibration of microchannel plate detector for carbon ions up to 250 MeV," J. Instrum. **14**, C04002–C04002 (2019).
[24]A. Mančić, J. Fuchs, P. Antici, S. A. Gaillard, and P. Audebert, "Absolute calibration of photostimulable image plate detectors used as (0.5-20 MeV) high-energy proton detectors," Rev. Sci. Instrum. **79**, 0–6 (2008).
[25]T. Bonnet, M. Comet, D. Denis-Petit, F. Gobet, F. Hannachi, M. Tarisien, M. Versteegen, and M. M. Aleonard, "Response functions of Fuji imaging plates to monoenergetic protons in the energy range 0.6-3.2 MeV," Rev. Sci. Instrum. **84**, 0–6 (2013).
[26]C. G. Freeman, G. Fiksel, C. Stoeckl, N. Sinenian, M. J. Canfield, G. B. Graeper, A. T. Lombardo, C. R. Stillman, S. J. Padalino, C. Mileham, T. C. Sangster, and J. A. Frenje, "Calibration of a Thomson parabola ion spectrometer and Fujifilm imaging plate detectors for protons, deuterons, and alpha particles," Rev. Sci. Instrum. **82**, 1–6 (2011).
[27]S. Kojima, T. Miyatake, S. Inoue, T. H. Dinh, N. Hasegawa, M. Mori, H. Sakaki, M. Nishiuchi, N. P. Dover, Y. Yamamoto, T. Sasaki, F. Ito, K. Kondo, T. Yamanaka, M. Hashida, S. Sakabe, M. Nishikino, and K. Kondo, "Absolute response of a Fuji BAS-TR imaging plate to low-energy protons (<0.2 MeV) and carbon ions (<1 MeV)," Rev. Sci. Instrum. **92**, 033306 (2021).
[28]N. Rabhi, D. Batani, G. Boutoux, J. E. Ducret, K. Jakubowska, I. Lantuejoul-Thfoin, C. Nauraye, A. Patriarca, A. Saïd, A. Semsoum, L. Serani, B. Thomas, and B. Vauzour, "Calibration of imaging plate detectors to mono-energetic protons in the range 1-200 MeV," Rev. Sci. Instrum. **88** (2017), 10.1063/1.5009472.
[29]I. J. Paterson, R. J. Clarke, N. C. Woolsey, and G. Gregori, "Image plate response for conditions relevant to laser-plasma interaction experiments," Meas. Sci. Technol. **19**, 095301 (2008).
[30]A. Alejo, S. Kar, H. Ahmed, A. G. Krygier, D. Doria, R. Clarke, J. Fernandez, R. R. Freeman, J. Fuchs, A. Green, J. S. Green, D. Jung, A. Kleinschmidt, C. L. S. Lewis, J. T. Morrison, Z. Najmudin, H. Nakamura, G. Nersisyan, P. Norreys, M. Notley, M. Oliver, M. Roth, J. A. Ruiz, L. Vassura, M. Zepf, and M. Borghesi, "Characterisation of deuterium spectra from laser driven multi-species sources by employing differentially filtered image plate detectors in Thomson spectrometers," Rev. Sci. Instrum. **85**, 0–7 (2014), 1408.2978.
[31]G. Boutoux, N. Rabhi, D. Batani, A. Binet, J. E. Ducret, K. Jakubowska, J. P. Nègre, C. Reverdin, and I. Thfoin, "Study of imaging plate detector sensitivity to 5-18 MeV electrons," Rev. Sci. Instrum. **86** (2015), 10.1063/1.4936141.
[32]D. O. Golovin, S. R. Mirfayzi, S. Shokita, Y. Abe, Z. Lan, Y. Arikawa, A. Morace, T. A. Pikuz, and A. Yogo, "Calibration of imaging plates sensitivity to high energy photons and ions for laser-plasma interaction sources," Journal of Instrumentation **16** (2021), 10.1088/1748-0221/16/02/T02005.
[33]D. Doria, S. Kar, H. Ahmed, A. Alejo, J. Fernandez, M. Cerchez, R. J. Gray, F. Hanton, D. A. MacLellan, P. McKenna, Z. Najmudin, D. Neely, L. Romagnani, J. A. Ruiz, G. Sarri, C. Scullion, M. Streeter, M. Swantusch, O. Willi, M. Zepf, and M. Borghesi, "Calibration of BAS-TR image plate response to high energy (3-300 MeV) carbon ions," Rev. Sci. Instrum. **86** (2015), 10.1063/1.4935582.
[34]J. Strehlow, P. Forestier-Colleoni, C. McGuffey, M. Bailly-Grandvaux, T. S. Daykin, E. McCary, J. Peebles, G. Revet, S. Zhang, T. Ditmire, M. Donovan, G. Dyer, J. Fuchs, E. W. Gaul, D. P. Higginson, G. E. Kemp, M. Martinez, H. S. McLean, M. Spinks, H. Sawada, and F. N. Beg, "The response function of fujifilm bas-tr imaging plates to laser-accelerated titanium ions," Review of Scientific Instruments **90**, 083302 (2019), https://doi.org/10.1063/1.5109783.
[35]T. Bonnet, M. Comet, D. Denis-Petit, F. Gobet, F. Hannachi, M. Tarisien, M. Versteegen, and M. M. Aléonard, "Response functions of imaging plates to photons, electrons and 4He particles," Rev. Sci. Instrum. **84**, 103510 (2013).
[36]http://www.srim.org.
[37]J. F. Ziegler, M. D. Ziegler, and J. P. Biersack, "SRIM - The stopping and range of ions in matter (2010)," Nucl. Instruments Methods Phys. Res. Sect. B Beam Interact. with Mater. Atoms **268**, 1818–1823 (2010).
[38]V. Lelasseux and J. Fuchs, "Modelling energy deposition in TR image plate detectors for various ion types," Journal of Instrumentation **15**, P04002–P04002 (2020).
[39]M. Nishiuchi, H. Sakaki, N. P. Dover, T. Miyahara, K. Shiokawa, S. Manabe, T. Miyatake, K. Kondo, K. Kondo, Y. Iwata, Y. Watanabe, and K. Kondo, "Ion species discrimination method by linear energy transfer measurement in Fujifilm BAS-SR imaging plate," Review of Scientific Instruments **91** (2020), 10.1063/5.0016515.
[40]J. B. Birks, "Scintillations from Organic Crystals: Specific Fluorescence and Relative Response to Different Radiations," Proc. Phys. Soc. A **64**, 874–877 (1951).
[41]T. Dzelzainis, G. Nersisyan, D. Riley, L. Romagnani, H. Ahmed, A. Bigongiari, M. Borghesi, D. Doria, B. Dromey, M. Makita, S. White, S. Kar, D. Marlow, B. Ramakrishna, G. Sarri, M. Zaka-Ul-Islam, M. Zepf, and C. L. S. Lewis, "The TARANIS laser: A multi-Terawatt system for laser-plasma investigations," Laser Part. Beams **28**, 451–461 (2010).

[42]M. Kanasaki, S. Jinno, H. Sakaki, K. Kondo, K. Oda, T. Yamauchi, and Y. Fukuda, "The precise energy spectra measurement of laser-accelerated MeV/n-class high-Z ions and protons using CR-39 detectors," Plasma Phys. Control. Fusion **58** (2016), 10.1088/0741-3335/58/3/034013.

[43]R. Prasad, D. Doria, S. Ter-Avetisyan, P. S. Foster, K. E. Quinn, L. Romagnani, C. M. Brenner, J. S. Green, P. Gallegos, M. J. V. Streeter, D. C. Carroll, O. Tresca, N. Dover, C. A. J. Palmer, J. Schreiber, D. Neely, Z. Najmudin, P. McKenna, M. Zepf, and M. Borghesi, "Calibration of Thomson parabola-MCP assembly for multi-MeV ion spectroscopy," Nucl. Instruments Methods Phys. Res. Sect. A Accel. Spectrometers, Detect. Assoc. Equip. **623**, 712–715 (2010).

[44]D. Doria, P. Martin, H. Ahmed, A. Alejo, M. Cerchez, S. Ferguson, J. Fernandez-Tobias, J. S. Green, D. Gwynne, F. Hanton, J. Jarrett, D. A. Maclellan, A. McIlvenny, P. McKenna, J. A. Ruiz, M. Swantusch, O. Willi, S. Zhai, M. Borghesi, and S. Kar, "Calibration of BAS-TR image plate response to GeV gold ions," Rev. Sci. Instrum. **93**, 033304 (2022).

[45]D. Jung, R. Hörlein, D. Kiefer, S. Letzring, D. C. Gautier, U. Schramm, C. Hübsch, R. Öhm, B. J. Albright, J. C. Fernandez, D. Habs, and B. M. Hegelich, "Development of a high resolution and high dispersion Thomson parabola," Rev. Sci. Instrum. **82** (2011), 10.1063/1.3523428.